Hindawi
Journal of Sensors
Volume 2018, Article ID 7323149, 11 pages
https://doi.org/10.1155/2018/7323149

Research Article

Intensity and Wavelength Division Multiplexing FBG Sensor System Using a Raman Amplifier and Extreme Learning Machine

Yibeltal Chanie Manie,[1] **Run-Kai Shiu**,[1] **Peng-Chun Peng**,[1] **Bao-Yi Guo**,[1] **Mekuanint Agegnehu Bitew**,[2] **Wei-Chieh Tang**,[1] **and Hung-Kai Lu**[1]

[1]*Department of Electro-Optical Engineering, National Taipei University of Technology, Taipei, Taiwan*
[2]*Department of Computer Science, Bahir Dar University, Bahir Dar, Ethiopia*

Correspondence should be addressed to Peng-Chun Peng; pcpeng@ntut.edu.tw

Received 13 April 2018; Accepted 11 July 2018; Published 13 September 2018

Academic Editor: Aftab M. Hussain

A fiber Bragg grating (FBG) sensor is a favorable sensor in measuring strain, pressure, vibration, and temperature in different applications, such as in smart structures, wind turbines, aerospace, industry, military, medical centers, and civil engineering. FBG sensors have the following advantages: immune to electromagnetic interference, light weight, small size, flexible, stretchable, highly accurate, longer stability, and capable in measuring ultra-high-speed events. In this paper, we propose and demonstrate an intensity and wavelength division multiplexing (IWDM) FBG sensor system using a Raman amplifier and extreme learning machine (ELM). We use an IWDM technique to increase the number of FBG sensors. As the number of FBG sensors increases and the spectra of two or more FBGs are overlapped, a conventional peak detection (CPD) method is unappropriate to detect the central Bragg wavelength of each FBG sensor. To solve this problem, we use ELM techniques. An ELM is used to accurately detect the central Bragg wavelength of each FBG sensor even when the spectra of FBGs are partially or fully overlapped. Moreover, a Raman amplifier is added to a fiber span to generate a gain medium within the transmission fiber, which amplifies the signal and compensates for the signal losses. The transmission distance and the sensing signal quality increase when the Raman pump power increases. The experimental results revealed that a Raman amplifier compensates for the signal losses and provides a stable sensing output even beyond a 45 km transmission distance. We achieve a remote sensing of strain measurement using a 45 km single-mode fiber (SMF). Furthermore, the well-trained ELM wavelength detection methods accurately detect the central Bragg wavelengths of FBG sensors when the two FBG spectra are fully overlapped.

1. Introduction

Fiber optic sensors are important in smart structures, mostly as a transmission line, as a sensing medium, or a combination of both. Fiber Bragg grating (FBG) is a favorable fiber optic sensor to measure strain, pressure, vibration, and temperature in different applications, such as in smart structures, wind turbines, aerospace, industry, military, medical centers, and civil engineering. In addition, applications of FBG sensors related to bridge monitoring, damage detection, structural health monitoring, railway transportation applications, and other harsh environment applications [1–3]. FBG sensors have the advantages of being immune to electromagnetic interference, light weight, small size, highly accurate, longer stability, and capable in measuring ultra-high-speed events. The sensing characteristics of FBG sensors involve identifying the variation of the central Bragg wavelength when it is subjected to physical parameters like vibration, strain, temperature, and other changes in the properties of the sensor [4–6]. Multiplexing of FBG sensors is an effective technology to deliver multipoint measurement along a single-fiber cable. Multiplexing reduces the operation and installation costs for quasidistributive strain measurements [7]. Among the various multiplexing techniques, wavelength division multiplexing (WDM) is an essential mechanism to recognize the exact central wavelength of each FBG sensor within the sensor network [7, 8]. In WDM, each FBG sensor needs a different Bragg wavelength and no

spectral overlap is allowed. However, the number of multiplexed sensors is restricted by both the broadband source bandwidth and the operating wavelength range required for each FBG sensor [9].

Recently, researchers have proposed intensity and wavelength division multiplexing (IWDM) techniques to increase the number of FBG sensors to be multiplexed [8–10]. IWDM has the advantage of low complexity. The IWDM scheme proposed in [9] used tunable fiber ring laser as a light source and a Fabry–Perot filter to select different wavelengths. However, this scheme is inappropriate for long-distance environment sensing, as it does not amplify the FBG signal. In [10], the authors proposed capacity and capability enhancement of the FBG sensor system using IWDM technique. However, IWDM has a problem of unmeasurable gap when two or more FBG spectra are partially or fully overlapped. Overlapping spectra cause crosstalk among the sensors and induce errors in central Bragg wavelength detection. Moreover, IWDM have a restriction on long-distance transmission when the number of FBG sensors increases. Nowadays, in addition to increasing the number of FBG sensors using IWDM, increasing the signal transmission distance is a very important issue.

In FBG sensor systems, the maximum signal transmission distance is commonly limited to 25 km due to signal loss in fiber link and Rayleigh scattering [11–16]. Moreover, signal loss and Rayleigh scattering induce optical noise and degrade the transmitted signal quality. Signal amplification is very important for long-distance transmission and remote sensing functionality. Among different optical signal amplification techniques, Raman amplification is the best amplifier to increase the transmission distance. Raman amplification entails generating a gain medium within the transmission fiber, which amplifies the signal before it reaches the optical receiver. Raman amplification has the capacity to amplify signals in any wavelength band using an appropriate pumping scheme [13–15]. By adding a Raman amplifier to a fiber span, signal power loss is decreased and it highly improves the signal-spontaneous beat noise performance. In order to realize a long-distance FBG sensor system, several approaches are proposed [13–17]. In [13], Raman laser for long-distance sensing has been demonstrated. However, FBGs are grouped together in the direction of the end of a long fiber, and consequently, the dynamic range of the interrogator is not possible to extend as it affects the response time of the system. Scheme [17] proposed linear-cavity fiber Raman laser for a long-distance FBG sensor system. The cavity consists of two FBGs connected to a fiber loop mirror. However, a fiber loop mirror has a limiting factor in system stability and configuration complexity. In addition, when strain is applied, the spectra of two FBGs might be overlapped and cannot address the sensing information of each FBG. Recently, besides increasing the number of FBG sensors and increasing the maximum transmission distance, much attention was focused on wavelength detection of spectrally overlapped FBG sensors.

In IWDM, central Bragg wavelength detection technique is a very important issue to detect each FBG central wavelength even when two or more FBG spectra are partially or fully overlapped [18]. Previous researchers have proposed several central wavelength detection methods, such as tabu-gradient search algorithm [18], filters [19, 20], conventional peak detection (CPD) [21], radial basis function network [22], and ADALINE network [23]. In [19], the sensing accuracy of FBG sensors was improved using a digital low-pass filter. However, the filter affects the measurement accuracy due to noise within the filter. CPD uses a tunable optical filter to detect the central wavelength of each FBG sensor [21]. However, this technique is inappropriate if the spectra of two or more FBGs are overlapped because it cannot address the sensing information of each FBG. All the above central wavelength detection methods have limitations on increasing the number of FBG sensors and detecting the central Bragg wavelength of FBGs when FBG spectra are overlapped.

This paper proposes a novel extreme learning machine (ELM) based central Bragg wavelength detection scheme for spectrally overlapped FBG sensors. An ELM accurately determines the central Bragg wavelengths. Compared to CPD machine learning methods, such as a neural network (NN) or support vector machine (SVM) [24], an ELM has the importance of good generalization and fast learning and requires less human intervention. An ELM is effective in real-time applications because it automatically determines all network parameters [25, 26]. Moreover, we propose IWDM to increase the number of FBG sensors and we employ a Raman amplifier to increase the sensing signal transmission distance and to improve the signal quality.

The rest of this paper is organized as follows. In Section 2, a brief discussion about operational principles with a mathematical expression is presented. Section 3 presents about an ELM. In Section 4, the experimental and simulation results are presented. Finally, we summarize the conclusion part of this paper in Section 5.

2. Operational Principles and Methods

The schematic diagram of applying IWDM and ELM techniques to a FBG sensor system is explained by using three FBG sensors as shown in Figure 1. A broadband light source is emitted from EDFA. The light emitted from the broadband light sources is injected into FBG sensors through a 2×2 coupler (50 : 50) and split into two branches (50 : 50). The one branch of a 50 : 50 coupler comprised a 1×2 coupler (30 : 70). The two FBG sensors (i.e., FBG1 and FBG2) are employed after a 30% and 70% output power ratio of a 1×2 coupler, respectively. FBG3 is employed after a 50% output power ratio of a 50 : 50 coupler. FBG3 is deployed after a 45 km SMF in order to have a gain medium. The back-reflected light from each FBG is propagated through the other arm of a 2×2 coupler and passes into the Raman amplifier. The Raman output power can be pumped to the SMF via a WDM coupler. The Raman amplifier consists of two laser diodes (LDs) with wavelengths of 1420 nm and 1450 nm. The polarization beam combiner (PBC) combines the outputs from the two LDs. The combined outputs from the two laser diodes are inserted into the Raman pump through the WDM coupler and the combined light is fed into a 45 km SMF. The output signal from the Raman amplifier is

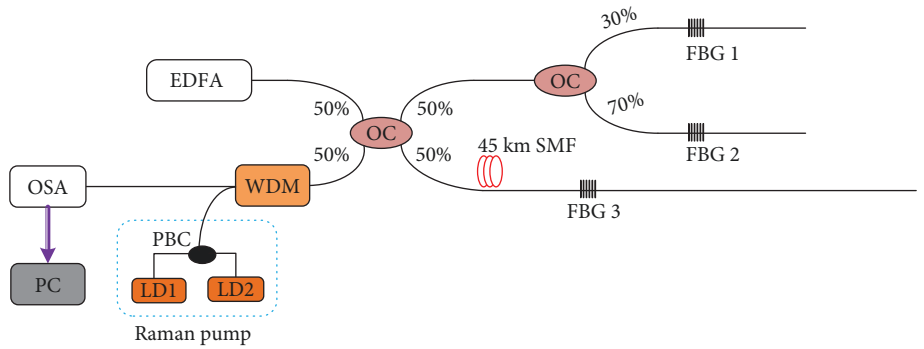

Figure 1: The schematic diagram of the proposed system (EDFA: erbium-doped fiber amplifier; OSA: optical spectrum analyzer; OC: optical coupler; FBG: fiber Bragg grating; SMF: single-mode fiber; WDM: wavelength division multiplexing; PBC: polarization beam combiner; LD: laser diode; PC: personal computer).

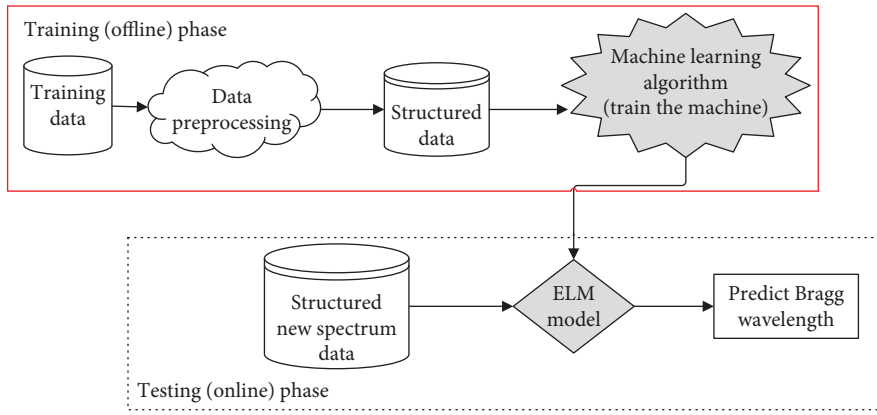

Figure 2: The architecture of ELM-based wavelength detection.

fed into the optical spectrum analyzer (OSA) to show the back-reflected wavelengths and to measure the central Bragg wavelengths. Finally, the measured reflected spectra of FBGs from OSA are sent to a personal computer (PC) for additional data processing.

The traditional WDM requires that each FBG sensor should have a unique spectral region, which limits the multiplexing capability of the sensor system [9]. The proposed method allows the reflection spectra of two FBGs which are overlapped when entering into the overlapping region. When a bandwidth of the full width at half maximum (FHWM) is larger than the distance between two FBG central wavelengths, it is difficult to identify each FBG central Bragg wavelength [24]. Hence, in our study, the central wavelength detection of overlapped spectra is converted to a regression problem. We assume that $R(\lambda)$ is the reflected spectra of FBGs from the OSA and λ_{Bi} $(i = 1, 2, 3)$ are the central Bragg wavelengths of the ith FBG. The measured spectra from the OSA are expressed as

$$R(\lambda, \lambda_B) = \left(\sum_{i}^{n} R_i g_i(\lambda, \lambda_{Bi}) \right) + \text{noise}(\lambda), \quad (1)$$

where $\lambda_B = [\lambda_{B1}, \lambda_{B2}, \lambda_{B3}]$ are the central Bragg wavelengths of FBGs, $R_i g_i(\lambda, \lambda_{Bi})$ is the peak reflectivity of the ith FBG, n is the number of FBG sensors, and noise (λ) is a random noise.

If the spectra of FBGs are overlapped, it is very difficult to determine the central Bragg wavelengths (λ_{Bi}) from the spectra $R(\lambda, \lambda_B)$ using CPD methods. Hence, we use ELM techniques to detect (identify) the central Bragg wavelength of each FBG sensor. The proposed ELM is employed to do multiple-input-multiple-output regression as shown in Figure 2. ELM is a supervised learning algorithm which has two different phases, that is, the training phase (offline phase) and testing phase (online phase). During the training phase, a number of training data are provided to train the ELM.

$$\text{Data} = \{(x_1, y_1), \ldots, (x_k, y_{k1}), \ldots, (x_n, y_n)\}, \quad (2)$$

where $x_k = R(\lambda) \in R^n$ is the sampling data from the FBG reflection spectra generated using (1), $y_k = \lambda_B \in R^m$ are the corresponding target outputs, n is the number of wavelengths in the spectra, and m is the number of FBG sensors in the system.

During the testing phase, only the new measured FBG reflection spectra from the OSA are fed into the well-trained ELM model. The well-trained ELM model quickly detects (identify) the central Bragg wavelengths of each FBG.

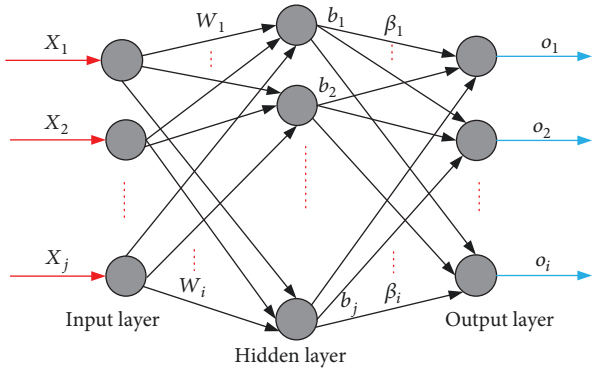

FIGURE 3: Structure of a single-hidden layer feedforward neural network (SLFN).

3. Extreme Learning Machine (ELM)

This paper proposes an ELM-based central Bragg wavelength detection to address the issue of a nonlinear relationship between FBG and strain factors. Scheme [24] proposed an ELM for single-hidden layer feedforward networks (SLFNs). A SLFN structure contains three layers, such as the input layer, hidden layer, and output layer, which are connected by neurons, as shown in Figure 3.This method is limited to feedforward neural networks with a single nonlinear hidden layer, as this type of network is capable of making a random close approximation of any continuous nonlinear mapping [27]. Instead of using traditional gradient-based learning methods which require several iterations, an ELM has its input weights randomly generated and uses simple matrix computations between hidden layers and output layers to determine the output weights. Solving the regularized least squares in ELM is faster than solving the quadratic programming problem in the SVM method [25, 26].

The ELM approach considers the wavelength detection problem as a regression problem. During the training process, the ELM randomly generates input weights w_i and bias values b_i. The prediction can be computed only by determining the activation function and the number of neurons in the hidden layer. Given the training data by (2), the standard SLFN for an arbitrary N different samples (x_j, t_j), where $x_j = [x_1, x_2, \dots, x_n]^T \in R^n$ is the input wavelength spectra and $t_j = [t_1, t_2, \dots, t_m]^T \in R^m$ is the target Bragg wavelength of FBGs. Standard SLFNs with activation function $g(x)$ and $\tilde{N}$ hidden neurons are mathematically expressed as follows:

$$\sum_{i=1}^{\tilde{N}} \boldsymbol{\beta}_i g(w_i \cdot x_j + b_i) = t_j, \quad i = 1, 2, \dots, N, \tag{3}$$

where $\boldsymbol{\beta}_i = [\beta_1, \beta_2, \dots, \beta_m]^T$ is the output weights connecting the ith hidden neuron and output neurons, $w_i = [w_1, w_2, \dots, w_n]^T$ is the randomly chosen input weights connecting the input neurons and the ith hidden neurons, $\tilde{N}$ is hidden neuron number, b_j is the random bias connecting the input layers and the ith hidden layer, and t_j is the actual outputs of input x_j.

According to [24], (3) can be rewritten into a matrix form as follows:

$$\mathbf{H}\boldsymbol{\beta} = \mathbf{T}, \tag{4}$$

where

$$\mathbf{H} = \begin{bmatrix} g(w_1 \cdot x_1 + b_1) & \dots & g(w_{\tilde{N}} \cdot x_1 + b_{\tilde{N}}) \\ \vdots & \cdots & \vdots \\ g(w_1 \cdot x_N + b_1) & \dots & g(w_{\tilde{N}} \cdot x_N + b_{\tilde{N}}) \end{bmatrix} N \times \tilde{N},$$

$$\boldsymbol{\beta} = \begin{bmatrix} \beta_1^T \\ \vdots \\ \beta_{\tilde{N}}^T \end{bmatrix} \tilde{N} \times m,$$

$$\mathbf{T} = \begin{bmatrix} t_1^T \\ \vdots \\ t_{\tilde{N}}^T \end{bmatrix} N \times m, \tag{5}$$

where $\mathbf{H}$ is the output matrix of hidden layers, $\boldsymbol{\beta}_i$ is the output weight matrix, and $\mathbf{T}$ is the target output. In backpropagation learning algorithm, a user requires specifying the value of the learning rate and the total error function will not be found. Backpropagation learning algorithm may overtrain and can have local minima [28]. To overcome this problem, scheme [28] proposed the smallest norm least squares solution of $\mathbf{H}\boldsymbol{\beta} = \mathbf{T}$. Thus, the output weight $\boldsymbol{\beta}$ can be calculated by the inner product of the matrix of $\mathbf{H}$ and $\mathbf{T}$ as the following [24].

$$\boldsymbol{\beta} = \mathbf{H}^+\mathbf{T}, \tag{6}$$

where $\boldsymbol{\beta}$ is the output weight matrix, $\mathbf{H}^+$ is the Moore-Penrose pseudoinverse (MPPI) of matrix $\mathbf{H}$ [29], and $\mathbf{T}$ is the target output. Equation (6) provides the best generalization performance with a minimum training error [28]. Finally, once $\boldsymbol{\beta}$ is obtained, the well-trained ELM can be used for regression task. When we obtain newly measured reflected overlap spectra of FBGs from the OSA as a testing sample data z_i, the equivalent outputs of the well-trained ELM can be mathematically calculated as

$$O_i = \sum_{i=1}^{\tilde{N}} \boldsymbol{\beta}_i g(w_i \cdot z_i + b_i), \quad i = 1, 2, \dots, N, \tag{7}$$

where O_i is the output of the ELM which is the detected (estimated) central Bragg wavelength of each FBG. Therefore, the well-trained ELM can detect or estimate the central wavelengths of the testing sample. Generally, the algorithm of the ELM network is a learning algorithm which is given a training set: $D = \{(x_j, t_j) \mid x_j \in R^n t_j \in R^m j = 1 \dots N\}$, activation function $g(w, b, x)$, and the number of

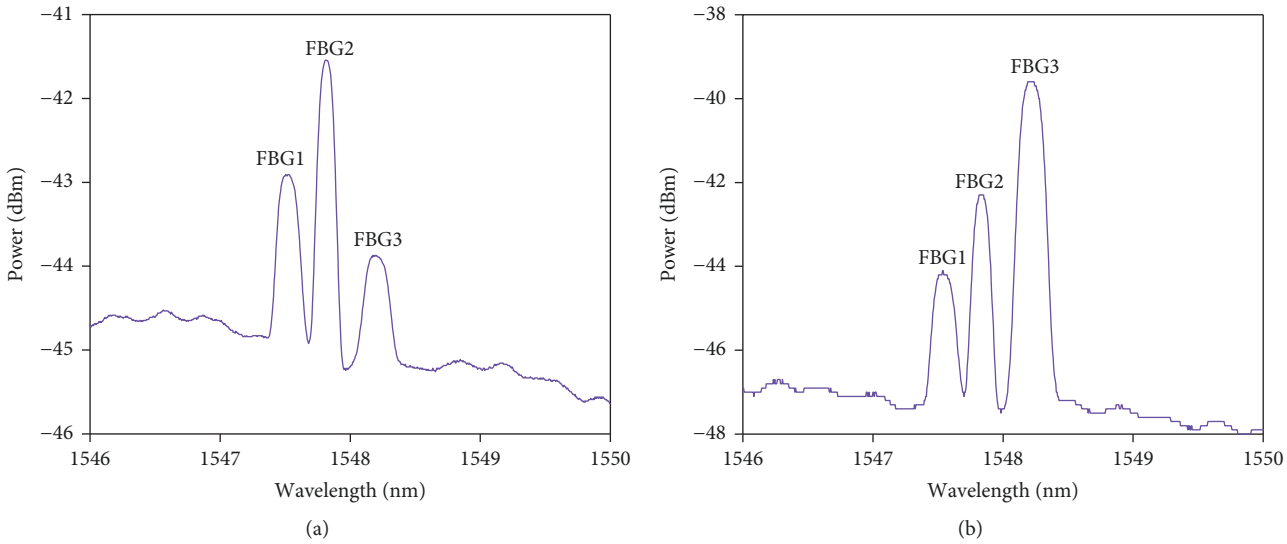

Figure 4: The measured spectra of three FBGs (a) before the Raman pump (b) after the Raman pump.

hidden nodes $\tilde{N}$. The ELM-based learning procedure can be summarized as follows:

(1) Determine the number of hidden layer neurons, randomly set bias b_i, and set weights w_i between the input layer and the hidden layer.

(2) Choose distinguishable activation function and then calculate output matrix $\mathbf{H}$ of the hidden layer for all the training samples.

(3) The weights b_i and the output weight $\boldsymbol{\beta} : \boldsymbol{\beta} = \mathbf{H}^{+}\mathbf{T}$ are calculated, where $\mathbf{H}^{+}$ is the MPPI of the hidden layer output matrix $\mathbf{H}$.

4. Experimental and Simulation Results

Figure 1 shows the experimental setup of the IWDM-FBG sensor system using a Raman amplifier and ELM. A broadband light source emitted from EDFA is injected into three FBG sensors. The measured reflection spectra of FBGs are sampled into 1001 points within a wavelength range from 1545.71 nm to 1550.71 nm. The span width of OSA is set to be 4 nm and the minimum resolution of the OSA is 0.03 nm. The measured reflection spectra of FBGs from the OSA are passed to a PC for further data processing. The central wavelengths of FBG1, FBG2, and FBG3 are 1547.54 nm, 1547.83 nm, and 1548.21 nm, respectively. The 3 dB bandwidths of the FBG1, FBG2, and FBG3 sensors are 0.24 nm, 0.226 nm and 0.24 nm, respectively. The reflectivity as well as bandwidth of the FBG sensors changes under different grating lengths and refractive index changes. We assumed that the reflection spectra of three FBGs are Gaussian shaped given by

$$R(\lambda, \lambda_{Bi}) = I_{\text{peak}} \exp\left[-4 \ln 2 * \left(\frac{\lambda - \lambda_{Bi}}{\Delta\lambda_{Bi}}\right)^2\right], \quad (8)$$

where λ is the wavelength, I_{peak} is the FBG maximum peak reflectivity, λ_{Bi} is the peak wavelength of FBGs, and $\Delta\lambda_{Bi}$ is the full width at half maximum. Typically, when the distance between three central Bragg wavelengths is smaller than the bandwidth of the full-width half maxima (FWHM), it is hard to directly distinguish each peak wavelength. The peak reflectivity of each FBG must be different to identify each FBG central Bragg wavelength from the overlapping spectra.

In the FBG sensor system, the maximum signal transmission distance is commonly limited to 25 km due to signal loss in fiber link and Rayleigh scattering. Signal loss and Rayleigh scattering induces optical noise and degrade the transmitted signal quality [11–16]. Therefore, we use a Raman amplifier to increase the transmission distance (long-distance sensing) and to compensate for the signal losses in long-distance transmission. As shown in Figure 1, FBG3 is deployed after 45 km SMF for long-distance signal transmission or for remote sensing up to 45 km. Figure 4(a) shows the measured spectra of three FBGs when the Raman pump is turned off. As shown in the figure, the power of FBG3 wavelength is very small and even disappears when the Raman pump is turned off. Hence, after 45 km transmission, it is very challenging to detect the central Bragg wavelength of FBG3 without employing a Raman amplifier. Therefore, by adding a Raman amplifier to a fiber span (FBG3), signal power loss is decreased and it highly improves the signal-spontaneous beat noise performance. Signal propagating along the fiber will be attenuated, but as it moves toward the fiber end where the Raman pump is located, it will start to experience some gain from the Raman pump wavelength. The higher power in the signal thus increases the signal-to-noise ratio (SNR), which enables longer fiber span, higher capacity and spectral efficiency, and longer distance. On the other hand, FBG1 and FBG2 have not been positioned in long distance compared to FBG3 as shown in Figure 1. Hence, FBG1 and FBG2 can sense signals below 25 km. As shown in Figure 4(a), the measured spectra of FBG1 and FBG2 are

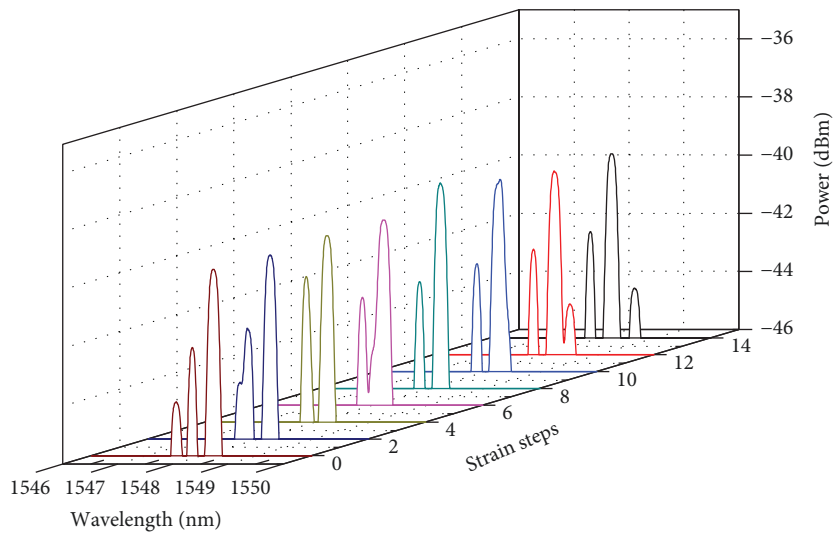

Figure 5: The reflected spectra of three FBG sensors using simulation when strain is applied to FBG1 corresponding to strain steps 0, 2, 4, 6, 8, 10, 12, and 14.

visible and can detect the central Bragg wavelength even when the Raman pump is turned off. Because of this, we do not need any Raman amplification in the FBG1 and FBG2 sensors. Figure 4(b) shows the measured spectra when the Raman pump is turned on. As shown in the figure, the sensing signal quality of FBG1 and FBG2 is the same with when the Raman pump is turned off. But, the sensing signal of FBG3 is significantly improved when the Raman pump is turned on because the Raman pump compensates for the signal loss of a long-distance fiber. After 45 km SMF transmission, the gain medium value of FBG3 before and after the Raman amplifier is 4 dB, which is adequate to compensate for the signal losses.

IWDM technique can increase the number of FBG sensors to be multiplexed by keeping the same dynamic range for each FBG sensor [8]. However, as the number of FBG sensors increases, the spectra of two or more FBGs are partially or fully overlapped. Hence, we use ELM to accurately determine the central Bragg wavelengths of each FGB when the spectra of two FBGs are overlapped. We develop a simulation environment using MATLAB to verify ELM-based central Bragg wavelength detection techniques when the spectra of FBGs are overlapped. The simulation runs on a PC, which has Intel Core i7-4790 3.60 GHz CPU and 20.48 GB RAM. The simulation of ELM-based central wavelength detection is conducted with three FBG sensors. Assume that the reflected spectra of three FBGs are Gaussian shaped [30]. The reflected spectra of three FBGs are added with random noise using (1) to simulate in a bad environment. During the simulation, the central Bragg wavelength of FBG1 is shifted from 1547.54 nm to 1548.662 nm by applying a changing strain to FBG1, while the Bragg wavelengths of FBG2 and FBG3 are fixed at 1547.83 nm and 1548.21 nm, respectively. The strain applied to FBG1 is increased by ~75 $\mu\varepsilon$ at each step. If a strain is applied to FBG1, the central Bragg wavelength will shift because the refractive index changes. Hence, the detected wavelength of FBG1 also shifts. The center Bragg wavelength shift of FBG1 according to the axial strain applied to a fiber grating is described as

$$\Delta\lambda B = \lambda B(1 - Pe)\varepsilon, \tag{9}$$

where $\Delta\lambda B$ is the central Bragg wavelength shift, λB is the central Bragg wavelength, Pe is the elastic-optical constant ($Pe \approx 0.22$), and ε is the applied strain to FBG1. If we know the central Bragg wavelength shift of FBG1 at each applied strain value, we can calculate the central Bragg wavelength of FBG1 at each applied strain value by using the following equation:

$$\lambda B = \frac{\Delta\lambda B}{(1 - Pe)\varepsilon}. \tag{10}$$

Therefore, we can change the central wavelength of FBG1 at each applied strain value using (1) and then the reflection spectra of FBGs are calculated by (1) using MATLAB simulation. The measurements are repeated for 14 different strain values (steps). Figure 5 shows the reflected spectra of three FBGs when a strain is applied to FBG1 corresponding to strain steps 0, 2, 4, 6, 8, 10, 12, and 14. As shown in the figure, it can be seen that the spectra of three FBGs are distinct at strain step 0, step 12, and step 14. But, the spectra of FBG1 and FBG2 are partially overlapped at strain step 2 and fully overlapped at strain step 4. Similarly, the spectra of FBG1 and FBG3 are partially overlapped at strain step 6 and step 10 and fully overlapped at strain step 8. As shown in Figure 6, the overlapping FBG spectra causes crosstalk and unmeasurable gaps between FBG sensors, which is why it is difficult to determine the exact central (peak) wavelength using the traditional CPD technique (without using ELM techniques).

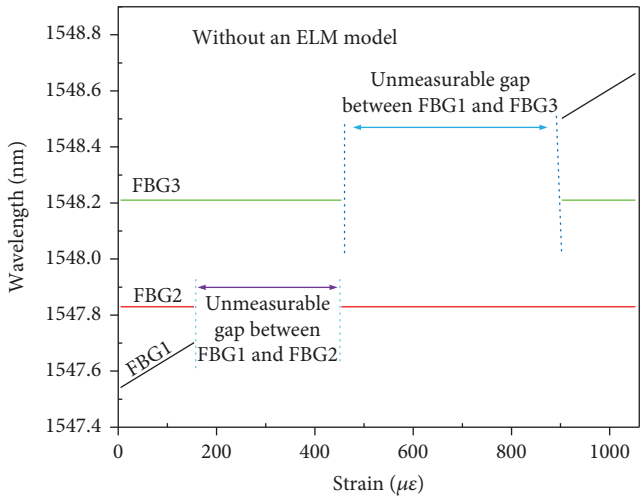

FIGURE 6: Unmeasurable gaps when the spectra of two FBG sensors are overlapped (i.e., without using an ELM model).

Figure 6 shows the unmeasurable gaps of three FBG sensors when the spectra of two FBGs are overlapped. We apply a strain within the range from 0 $\mu\varepsilon$ to 1052 $\mu\varepsilon$ to FBG1, and this causes its central wavelength to shift from 1547.54 nm to 1548.662 nm. When the applied strain to FBG1 is between 150 $\mu\varepsilon$ and 450 $\mu\varepsilon$, the spectra of FBG1 and FBG2 are overlapped and we cannot detect the central wavelengths of the two FBG sensors using CPD technique. The range that cannot detect the central wavelength of FBGs is called unmeasurable gaps. When the applied strain to FBG1 is greater than 450 $\mu\varepsilon$, the spectra of FBG1 and FBG2 are separated but the spectra of FBG1 are overlapped with FBG3. Applying a strain to FBG1 within the range of 450 $\mu\varepsilon$–900 $\mu\varepsilon$ will create unmeasurable gaps for both FBG1 and FBG3. Hence, we cannot detect the central wavelengths of FBG1 and FBG3 using CPD techniques. We can directly detect all the three FBG central Bragg wavelengths using CPD technique only if the applied strain is less than 150 $\mu\varepsilon$ or greater than 900 $\mu\varepsilon$. When the applied strain is between 150 $\mu\varepsilon$ and 900 $\mu\varepsilon$, unmeasurable gaps will be created for at least in the two FBG sensors. Because of this, we have proposed ELM to solve the overlapping or unmeasurable gap problem subsequently. For each applied strain value, the well-trained ELM can accurately detect the central Bragg wavelengths of three FBGs using (8) even when the spectra of FBGs are within the overlapping or unmeasurable gap range.

The proposed ELM techniques is demonstrated and tested by using MATLAB simulation to verify the feasibility of an ELM for wavelength detection mechanisms. In order to train an ELM, the training dataset are generated using (1), which is the reflection spectra of three FBGs by applying a changing strain to FBG1. The measurements are repeated for 14 different strain values (steps), and the reflection spectra of FBGs are calculated by (1) using MATLAB simulation. Figure 5 shows the reflection spectra of three FBGs when we apply different strains to FBG1.The training dataset has inputs and corresponding targets. The inputs are the reflection spectra of three FBGs at each applied strain value to FBG1, and the corresponding targets are the central wavelength of each FBG at each applied strain value to FBG1. The generated training data can be preprocessed and prepared to be used for training an ELM based on (2). The sample size of training data is 15000. ELM is trained for 30 times with the training datasets using feedforward neural network algorithms. During the training phase, we have adjusted the number of neurons, number of epochs, and the number of hidden layers to get the best generalization performance of the ELM. The best performance of the well-trained ELM is obtained when the number of neurons is 2000 and the number of epochs is 1000. The training and testing accuracy increases when the number of neurons increases. The test dataset is generated from the reflection spectra of three FBGs measured by an OSA using an experimental method. During the experiment, strain is applied to FBG1 to shift the central Bragg wavelength from 1547.54 nm to 1548.662 nm, while the central Bragg wavelengths of FBG2 and FBG3 are fixed. To apply a strain to FBG1, FBG1 is mounted on a translation stage (TS). Then, by manually tuning the TS, a strain is applied to FBG1. This manual tuning of the TS in the fiber grating leads to a shift in the central Bragg wavelength of FBG1. When the central Bragg wavelength of FBG1 shifts, an overlap occurs between FBG1 and FBG2 and between FBG1 and FBG3 at a different time. The shift in the central Bragg wavelength of FBG1 is observed and obtained from an OSA. The applied strain to FBG1 at each step is ~75 $\mu\varepsilon$. The strain (ε) is related to the displacement (ΔL) of the translation stage by $\varepsilon = \Delta L/L$, where L is the total fiber length under strain. After the strain is applied to FBG1, the reflection spectra of three FBGs are measured by using an OSA. The measurements are repeated for 14 different strain values (steps). For each applied strain value, three measurements are carried out within a period of 3 minutes. The sample size of testing data is 2000. Figures 7(a) and 7(b) show the reflection spectra of three FBGs generated by the OSA for some typical applied strain values (steps) to FBG1 corresponding to strain steps 4 and 8, respectively. During the test phase, we have taken new fully overlapped spectra from the OSA, as shown in Figures 7(a) and 7(b), to test the well-trained ELM model. The well-trained ELM model can accurately detect or determine the central Bragg wavelengths of FBG1, FBG2, and FBG3 by (8).

Figures 7(a) and 7(b) show the reflected spectra of three FBGs measured by an OSA by applying a strain to FBG1 corresponding to strain steps 4 and step 8, respectively. As shown in the figure, the two FBG sensor spectra are overlapped, which is why it is difficult to identify the central Bragg wavelength of each FBG using traditional CPD techniques. Therefore, we use ELM techniques to solve this problem. For each applied strain, an ELM achieved to obtain the exact central Bragg wavelengths of FBG1, FBG2, and FBG3 in all independent test runs. Figure 8 shows the simulation output of the detected central Bragg wavelengths of three FBGs using the well-trained ELM model when the spectra of FBG1 and FBG2 are fully overlapped at strain step 4 (see Figure 7(a)). The absolute value of the difference between the predicted central wavelength value and actual central wavelength values is calculated as the detection error, expressed as detection error = |predicted central wavelength

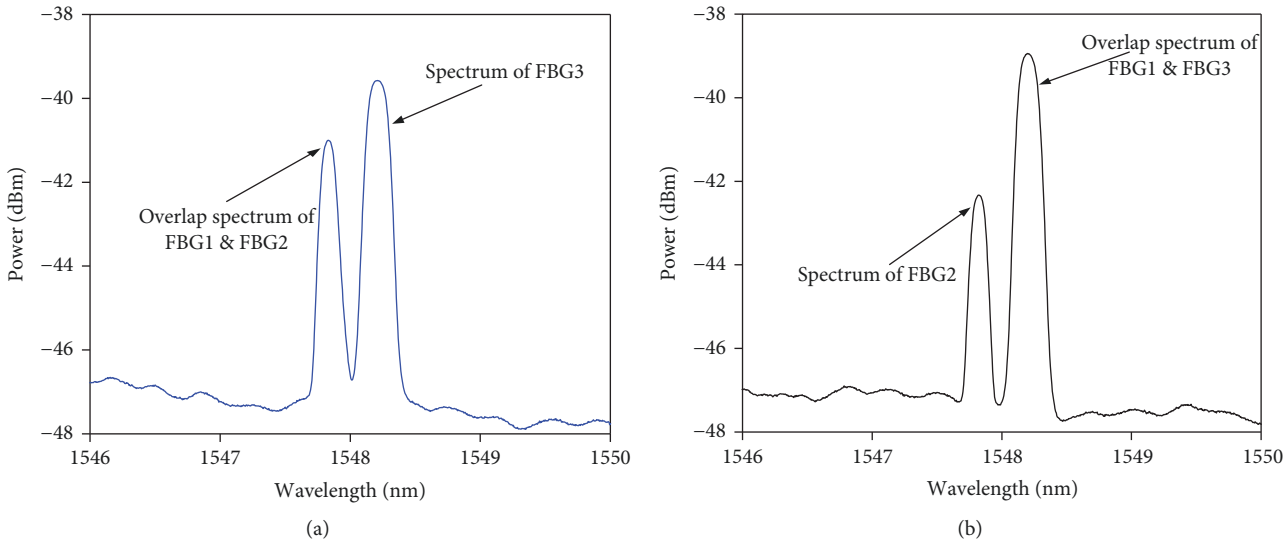

Figure 7: The reflected spectra of three FBG sensors from OSA (a) when the spectra of FBG1 and FBG2 are fully overlapped at strain step 4 (b) when the spectra of FBG1 and FBG3 are fully overlapped at strain step 8.

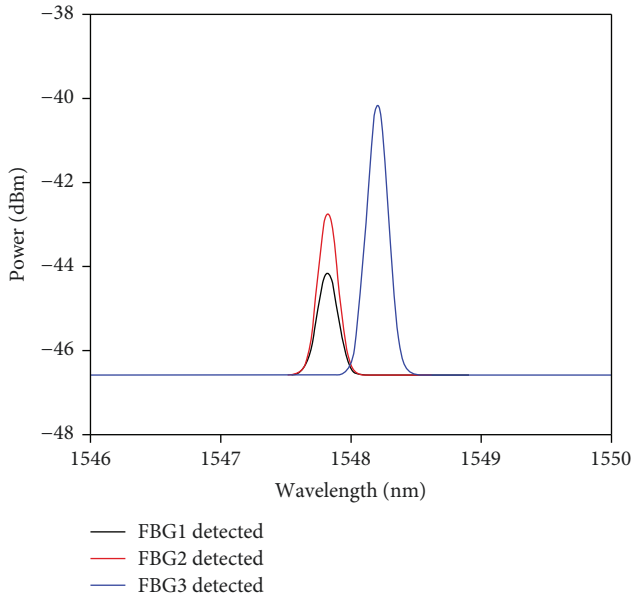

Figure 8: Output of the ELM model (the detected Bragg wavelengths of three FBGs when FBG1 and FBG2 are overlapped at strain step 4 using an ELM model).

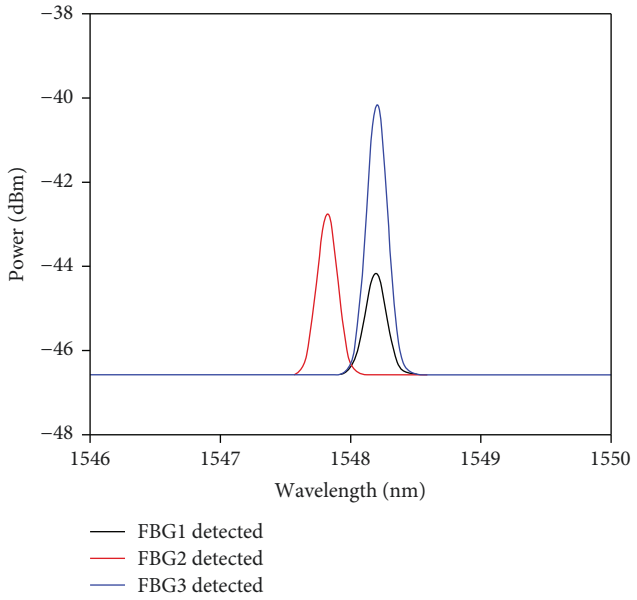

Figure 9: Output of the ELM model (the detected central Bragg wavelengths of three FBGs when FBG1 and FBG3 are overlapped at strain step 8 using an ELM model).

value – actual central wavelength values|. The detection error of the proposed ELM model when FBG1 and FBG2 spectra are overlapped is 0.018, which is a very small error. This indicates that we can accurately identify the central Bragg wavelengths of FBG1 and FBG2 even though the input spectra of the two FBG sensors are fully overlapped. Similarly, Figure 9 shows the simulation output of the detected central Bragg wavelengths of three FBGs using the well-trained ELM when the spectra of FBG1 and FBG3 are fully overlapped at strain step 8 (see Figure 7(b)). The detection error of the proposed method when FBG1 and FBG3 spectra are overlapped is 0.021, which is a very small error. Because the central wavelengths of FBG2 and FBG3 are fixed (constant), we can easily identify which central wavelength is for FBG1, FBG2, and FBG3 when the well-trained ELM detects (identify) the central wavelengths of three FBGs (see Figures 8 or 9). Only the FBG1 central wavelength varies during wavelength shift or overlap. Therefore, Figures 8 and 9 indicate that the well-trained ELM model can accurately detect the central Bragg wavelengths of FBG1, FBG2, and FBG3 even though the input spectra of the two FBG sensors are fully overlapped.

Figure 10 shows the output of the well-trained ELM model, which is the detected central Bragg wavelengths of three FBGs at each strain value (steps). When the central Bragg wavelengths of two FBGs are partially or fully overlapped (from strain step 2 to step 12), the proposed ELM

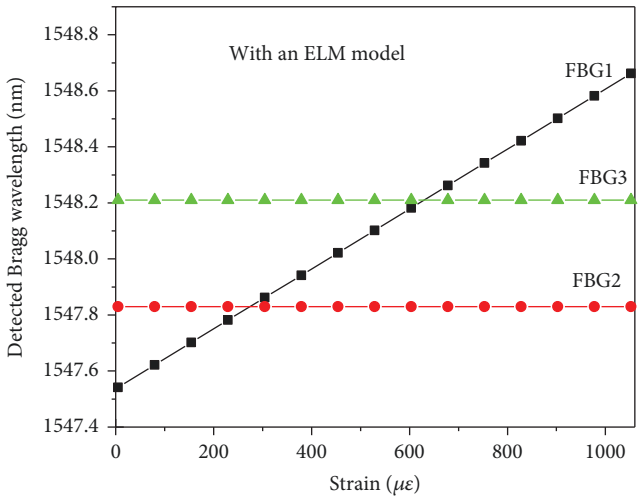

Figure 10: The detected central Bragg wavelengths of three FBGs at different strain values by using an ELM model.

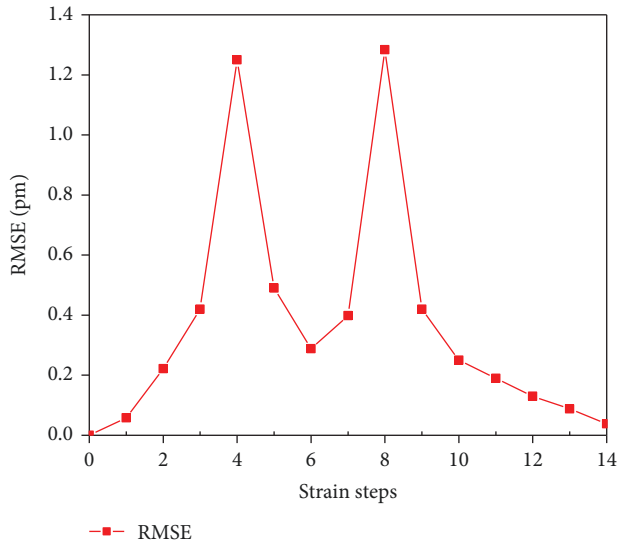

Figure 11: Performance of the proposed ELM model at each applied strain step.

can determine the central Bragg wavelengths of three FBGs even in the overlapping wavelength range. The performance of the ELM model can be described in terms of training time, testing time, and root-mean-square error (RMSE) values of the testing result. An ELM has an enormous advantage in training time and learning speed. When the number of hidden neurons is 2000, the training time of the ELM is 12 s and the testing time of the ELM is 0.10 s. Both the training time and testing time increase when the number of hidden neurons increases. Since an ELM model can directly determine the central Bragg wavelengths of FBG sensors, an ELM is much simpler and greatly reduces the training time and testing time than CPD techniques. RMSE can evaluate the central Bragg wavelength detection performance of the well-trained ELM when two or more FBG spectra are partially or fully overlapped. RMSE values can be calculated by the following equation:

$$\text{RMSE} = \sqrt{\frac{\sum_{i=1}^{n} (P_i - A_i)^2}{n}}, \tag{11}$$

where A_i is the actual central Bragg wavelength, P_i is the predicted (detected) central Bragg wavelength, and n is the number of test data. The central Bragg wavelength detection accuracy of the well-trained ELM model in terms of RMSE throughout the operation strain range (from 0 to 1052 $\mu\varepsilon$) is 0.3 pm.

Figure 11 shows the well-trained ELM central Bragg wavelength detection errors (i.e., RMSE) against 14 strain steps. As shown in the figure, the RMS error is very high when the two FBG spectra is fully overlapped (when strain step = 4 and step = 8) which means that the detection accuracy decreases when the two wavelength spectra are overlapped. When the two central Bragg wavelengths fully overlapped (at strain step = 4 and step = 8), an ELM can identify the central Bragg wavelengths of three FBGs. The RMS error in strain step 4 and step 8 is 1.25 pm and 1.28 pm, respectively. Figure 12 shows the RMS errors with epochs. The detection performance of an ELM is stable when the number of epoch increases, but it tends to become worse when too few epochs are used. As shown in the figure when the epoch number is 1000, the RMS error becomes around 0.25 pm which is very small. Therefore, experimental and simulation results show, using the well-trained ELM, that the central Bragg wavelengths of FBGs are identified with definite accuracy, even if the reflected spectra of FBGs are fully overlapped. The central Bragg wavelength detection accuracy achieved by an ELM is 0.3 pm, which has better generalization performance than CPD techniques [19–23].

5. Conclusion

This paper introduces an IWDM-FBG sensor system using a Raman amplifier and ELM. FBGs are favorable sensors in different applications and have the advantages of being immune to electromagnetic interference, light weight, flexible, stretchable, small size, highly accurate, longer stability, and capable in measuring ultra-high-speed events. A Raman amplifier is used to increase the sensing signal transmission distance and optimize the quality of the signal. Increasing the Raman pump power increases the transmission distance and the sensing signal quality. The experimental result revealed that a Raman amplifier can compensate for the signal losses and can provide a stable sensing output even beyond a 45 km transmission distance. Moreover, we achieve a remote sensing of strain measurement at a remote location of 45 km. We employed IWDM to increase the number of FBG sensors and to allow FBG spectra to overlap. The proposed ELM can address the problem of the unmeasurable gaps that have been faced in IWDM techniques. ELM is much simpler, greatly reduces the training time and testing time, and improves the detection accuracy than convolutional wavelength detection techniques. The RMSE of the proposed system is 0.3 pm which is possible to accurately

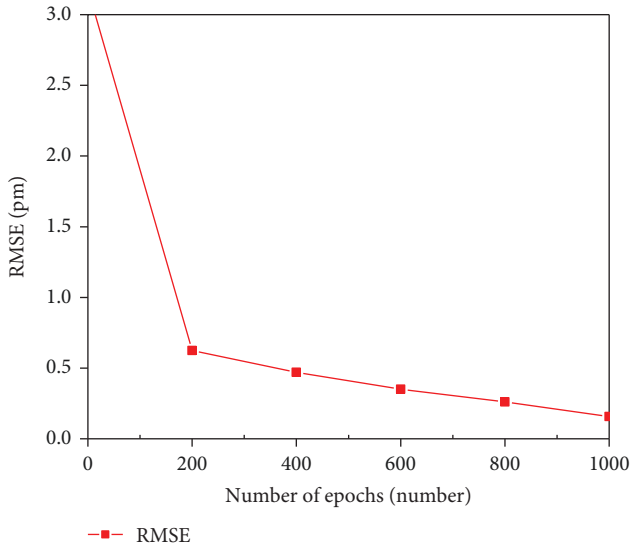

Figure 12: Performance of the proposed ELM model on a number of epochs.

detect the central Bragg wavelengths of each FBG even if the spectra of FBGs are fully overlapped.

Data Availability

The data used to support the findings of this study are available from the first author upon request.

Conflicts of Interest

The authors declare that there is no conflict of interest regarding the publication of this paper.

Acknowledgments

This work was supported by the Ministry of Science and Technology, Taiwan, under Contract MOST 106-2221-E-027-100.

References

[1] R. Kashyap, *Fiber Bragg Gratings*, Academic Press, New York, NY, USA, 2009.

[2] A. D. Kersey, M. A. Davis, H. J. Patrick et al., "Fiber grating sensors," *Journal of Lightwave Technology*, vol. 15, no. 8, pp. 1442–1463, 1997.

[3] J. Cui, Y. Hu, K. Feng, J. Li, and J. Tan, "FBG interrogation method with high resolution and response speed based on a reflective-matched FBG scheme," *Sensors*, vol. 15, no. 7, pp. 16516–16535, 2015.

[4] H. F. Lima, P. F. Antunes, J. D. L. Pinto, and R. N. Nogueira, "Simultaneous measurement of strain and temperature with a single fiber Bragg grating written in a tapered optical fiber," *IEEE Sensors Journal*, vol. 10, no. 2, pp. 269–273, 2010.

[5] C. C. Ma and C. W. Wang, "Transient strain measurements of a suspended cable under impact loadings using fiber Bragg grating sensors," *IEEE Sensors Journal*, vol. 9, no. 12, pp. 1998–2007, 2009.

[6] Z. Zhang, L. Yan, W. Pan et al., "Sensitivity enhancement of strain sensing utilizing a differential pair of fiber Bragg gratings," *Sensors*, vol. 12, no. 4, pp. 3891–3900, 2012.

[7] K. S. Choi, J. Youn, E. You et al., "Improved spectral tag method for FBG sensor multiplexing with equally spaced spectral codes and simulated annealing algorithm," in *2009 IEEE Sensors*, pp. 1256–1259, Christchurch, New Zealand, 2009.

[8] L. Zhang, Y. Liu, J. A. R. Williams, and I. Bennion, "Enhanced FBG strain sensing multiplexing capacity using combination of intensity and wavelength dual-coding technique," *IEEE Photonics Technology Letters*, vol. 11, no. 12, pp. 1638–1640, 1999.

[9] P. C. Peng, J. H. Lin, H. Y. Tseng, and S. Chi, "Intensity and wavelength-division multiplexing FBG sensor system using a tunable multiport fiber ring laser," *IEEE Photonics Technology Letters*, vol. 16, no. 1, pp. 230–232, 2004.

[10] C. H. Yeh, Y. H. Zhuang, N. Tsai, and C. W. Chow, "Capacity and capability enhancements of FBG sensor system by utilizing intensity and WDM detection technique," *Smart Materials and Structures*, vol. 26, no. 3, article 035026, 2017.

[11] H. Y. Fu, H. L. Liu, W. H. Chung, and H. Y. Tam, "A novel fiber Bragg grating sensor configuration for long-distance quasi-distributed measurement," *IEEE Sensors Journal*, vol. 8, no. 9, pp. 1598–1602, 2008.

[12] S. K. Liaw, Y. W. Lee, H. W. Huang, and W. F. Wu, "Multi-wavelength linear-cavity SOA-based laser array design for multiparameter and long-haul sensing," *IEEE Sensors Journal*, vol. 15, no. 6, pp. 3353–3358, 2015.

[13] Y. G. Han, T. V. A. Tran, S. H. Kim, and S. B. Lee, "Multiwavelength Raman-fiber-laser-based long-distance remote sensor for simultaneous measurement of strain and temperature," *Optics Letters*, vol. 30, no. 11, pp. 1282–1284, 2005.

[14] Y. G. Han, T. V. A. Tran, S. H. Kim, and S. B. Lee, "Development of a multiwavelength Raman fiber laser based on phase-shifted fiber Bragg gratings for long-distance remote-sensing applications," *Optics Letters*, vol. 30, no. 10, pp. 1114–1116, 2005.

[15] Y. Nakajima, Y. Shindo, and T. Yoshikawa, "Novel concept as long-distance transmission FBG sensor system using distributed Raman amplifier," in *Proceedings of the 16th International Conference on Optical Fiber Sensor (OFS) Th1-4*, pp. 530–533, Nara, Japan, October 2003.

[16] B. Y. Guo, W. C. Tang, Y. C. Manie, M. A. Bitew, H. K. Lu, and P. C. Peng, "Long-distance sensing fiber sensor system using broadband source and Raman amplifier," in *2017 IEEE International Conference on Consumer Electronics - Taiwan (ICCE-TW)*, pp. 413-414, Taipei, Taiwan, 2017.

[17] P. C. Peng, H. Y. Tseng, and S. Chi, "Long-distance FBG sensor system using a linear-cavity fiber Raman laser scheme," *IEEE Photonics Technology Letters*, vol. 16, no. 2, pp. 575–577, 2004.

[18] X. Xu, J. Chicharo, and J. Xi, "Improving the performance of IWDM FBG sensing system using tabu-gradient search algorithm," in *2006 International Symposium on Intelligent Signal Processing and Communications*, pp. 788–791, Tottori, Japan, 2006.

[19] C. C. Chan, W. Jin, and M. S. Demokan, "Enhancement of measurement accuracy in fiber Bragg grating sensors by using digital signal processing," *Optics & Laser Technology*, vol. 31, no. 4, pp. 299–307, 1999.

[20] C. C. Chan, J. M. Gong, C. Z. Shi et al., "Improving measurement accuracy of fiber Bragg grating sensor using digital

matched filter," *Sensors and Actuators A: Physical*, vol. 104, no. 1, pp. 19–24, 2003.

[21] E. Udd, "Fiber optic smart structures," *Proceedings of the IEEE*, vol. 84, no. 6, pp. 884–894, 1996.

[22] A. S. Paterno, J. C. C. Silva, M. S. Milczewski, L. V. R. Arruda, and H. J. Kalinowski, "Radial-basis function network for the approximation of FBG sensor spectra with distorted peaks," *Measurement Science and Technology*, vol. 17, no. 5, pp. 1039–1045, 2006.

[23] C. C. Chan, C. Z. Shi, W. Jin, and D. N. Wang, "Improving the wavelength detection accuracy of FBG sensors using an ADALINE network," *IEEE Photonics Technology Letters*, vol. 15, no. 8, pp. 1126–1128, 2003.

[24] G. B. Huang, Q. Y. Zhu, and C. K. Siew, "Extreme learning machine: theory and applications," *Neurocomputing*, vol. 70, no. 1–3, pp. 489–501, 2006.

[25] X. Chen, Z. Y. Dong, K. Meng, Y. Xu, K. P. Wong, and H. W. Ngan, "Electricity price forecasting with extreme learning machine and bootstrapping," *IEEE Transactions on Power Systems*, vol. 27, no. 4, pp. 2055–2062, 2012.

[26] R. Rajesh and J. S. Prakash, "Extreme learning machines-a review and state-of-the-art," *International Journal of Wisdom Based Computing*, vol. 1, no. 1, pp. 35–39, 2011.

[27] F. Han, D. S. Huang, Z. H. Zhu, and T. H. Rong, "The forecast of the postoperative survival time of patients suffered from non-small cell lung cancer based on PCA and extreme learning machine," *International Journal of Neural Systems*, vol. 16, no. 1, pp. 39–46, 2006.

[28] M. Pal, "Extreme-learning-machine-based land cover classification," *International Journal of Remote Sensing*, vol. 30, no. 14, pp. 3835–3841, 2009.

[29] D. Serre, *Matrices: Theory and Applications*, Springer-Verlag, New York, NY, USA, 2010.

[30] C. Z. Shi, N. Zeng, C. C. Chan, Y. B. Liao, W. Jin, and L. Zhang, "Improving the performance of FBG sensors in a WDM network using a simulated annealing technique," *IEEE Photonics Technology Letters*, vol. 16, no. 1, pp. 227–229, 2004.